Journal of Applied Polymer Science

Synergistic Effect of Dopant Combination and Switchover in Formation Mechanism of Polyaniline Nanowire

Subhendu Bhandari, Dipak Khastgir
Rubber Technology Centre, Indian Institute of Technology Kharagpur, Kharagpur 721302, West Bengal, India
Correspondence to: D. Khastgir (E-mail: khasdi@rtc.iitkgp.ernet.in)

ABSTRACT: Self-assembled polyaniline (PAni) was synthesized electrochemically in dimethylformamide medium to study the effect of simultaneous use of organic–inorganic dopant combination in aprotic polar synthesis medium. During the synthesis process, simultaneous dual doping was performed using *p*-toluenesulfonic acid and sulfuric acid with varying the ratio of the dopants keeping their total concentration unchanged. Nanowire meshes were formed where switchover in nanostructure formation is observed. Nanowire in individually doped PAni was formed with directional joining of smaller nanoparticles or from multilayered tubular nanostructures whereas, for dual doped PAni, either of these two was observed. Periodicity parallel and perpendicular to polymer chain were found in well correlation with diameter of nanowires. Synergistic improvements in AC conductivity, specific capacitance, and thermal degradation within certain temperature range were observed in particular ratio of the dopants. © 2014 Wiley Periodicals, Inc. J. Appl. Polym. Sci. **2015**, *132*, 41520.

KEYWORDS: conducting polymers; dual doping; electropolymerization; nanostructured polymers; self-assembly

Received 11 June 2014; accepted 12 September 2014
DOI: 10.1002/app.41520

INTRODUCTION

Control of morphology in self-assembled nanostructured polymer is challenge in the field of nanoscience. Differences in morphological texture of any polymer synthesized in different conditions are widely reported. Apart from that, the formation of similar nanowires from different assembly motifs at nanoscale may add new direction in the morphological aspect. Intrinsically conducting polymers (ICP) show wide range of morphology[1–4] under different synthesis conditions. Polyaniline (PAni) is an important member of ICP family. It can be a useful component in potential applications like supercapacitor,[5,6] gas sensor,[7–9] corrosion inhibitor,[10] EMI shielding,[11] and so forth, owing to its wide range of electrical conductivity, environmental stability, low cost of synthesis, and so forth. PAni can be synthesized in different methods, for example, oxidative polymerization process,[12] electrochemical polymerization,[13] interfacial polymerization,[14] solid state polymerization (mechanochemical),[15] and so forth. Properties of PAni vary with process parameters.[16,17] Electrical conductivity of PAni depends on oxidation state, doping level, and type of dopant. Doping with inorganic as well as organic acids enhances its conductivity.[2,18] Organic and inorganic acids may be used individually[19,20] or simultaneously[21] to prepare electrochemical capacitors. Doping method is crucial for its structure and properties. In secondary doping method, a suitable organic solvent[22] or specially an apparently "inert" material,[23] for example, *m*-cresol is used as secondary dopant where conventional dopant acts as primary dopant. In dual doping process, two dopants are used one after another.[24] Conversely, two dopants are used at the same time during synthesis of PAni in simultaneous dual doping process where synergy in electrical property may also be achieved.[25] Early reports revealing the formation of different nano and microstructures like rod,[26] sphere,[27] wire,[28] tube,[29] flake,[30] rice-grain,[31] and so forth, in PAni raise the interest about possible formation and transformation mechanism of the morphological structures. In our previous investigation using simultaneous dual doping process in electropolymerization, it has been found that different nanostructured PAni agglomerated to form similar macrospheres.[25] In this work, we have explored switchover in formation mechanism of similar self-assembled nanowires from different nanostructures, which is akin to transformation of multilayers or nanoparticles to tubular structure instead of mere agglomeration as reported in the previous work using the same dopant combination. Earlier report[32] reveals the transformation of layer to tubular nanostructure in supramolecular assembly by tuning the stability of the hydrophilic edges in polar/non-polar solvents. However, the layer-to-tubular transformation has been observed in this work by varying the ratio of dopants without changing the polarity of the solvent. Although, most of the reports on polyaniline follow the synthesis procedure in

© 2014 Wiley Periodicals, Inc.

Table I. Sample Designations of Synthesized PAni

Sample code	Concentration of H_2SO_4	Concentration of PTSA	$[H_2SO_4]$: [PTSA]	Types of synthesized PAni
PS_4T_0	1*M*	0	4 : 0 (=1 : 0)	Individually doped
PS_3T_1	0.75*M*	0.25*M*	3 : 1	Dual doped
PS_2T_2	0.5*M*	0.5*M*	2 : 2 (=1 : 1)	Dual doped
PS_1T_3	0.25*M*	0.75*M*	1 : 3	Dual doped
PS_0T_4	0	1*M*	0 : 4 (=0 : 1)	Individually doped

aqueous medium, the structure–property relationship for synthesis in any other medium is also becoming nowadays a subject of interest. Simultaneous doping of PAni with *p*-toluenesulfonic acid (PTSA) in dimethylformamide (DMF) medium was investigated by Roy et al.[33] where synthesis process involved relatively higher voltage, whereas our study reveals the formation of multilayered structure of PAni with PTSA doping using very low current flow during the synthesis. Although the effect of codopant in enhancement of conductivity of polyaniline synthesized in DMF medium via chemical polymerization method has recently been reported,[34] here conventional secondary doping does not reveal any synergistic effect of dopants at constant total dopant concentration. In this context, simultaneous dual doping of polyaniline in DMF medium may give an insight into the working of the dopant combination in aprotic polar medium. This investigation has explored the use of inorganic–organic acid combination of sulfuric acid (H_2SO_4) and *p*-toluene sulfonic acid (PTSA) at constant dopant concentration for doping of PAni during its electrochemical synthesis. Apart from morphological transformation, synergistic improvements in AC conductivity, specific capacitance, and thermal stability within certain range have been observed for some particular dopant ratio. Thus, the synergistic effect of the dopant combination has been established for synthesis of PAni in aprotic polar medium.

EXPERIMENTAL

Materials

Analytical grade aniline, dimethylformamide, sulfuric acid (98%), methanol, and ethanol were obtained from Merk, India. PTSA was obtained from Spectrochem, India. All the materials were used as received. Graphite plate (14.5 cm × 5 cm × 0.5 cm) working electrode and copper plate (15 cm × 5 cm × 0.05 cm) counter electrode were used in electropolymerization. For filtration, deionized water was used.

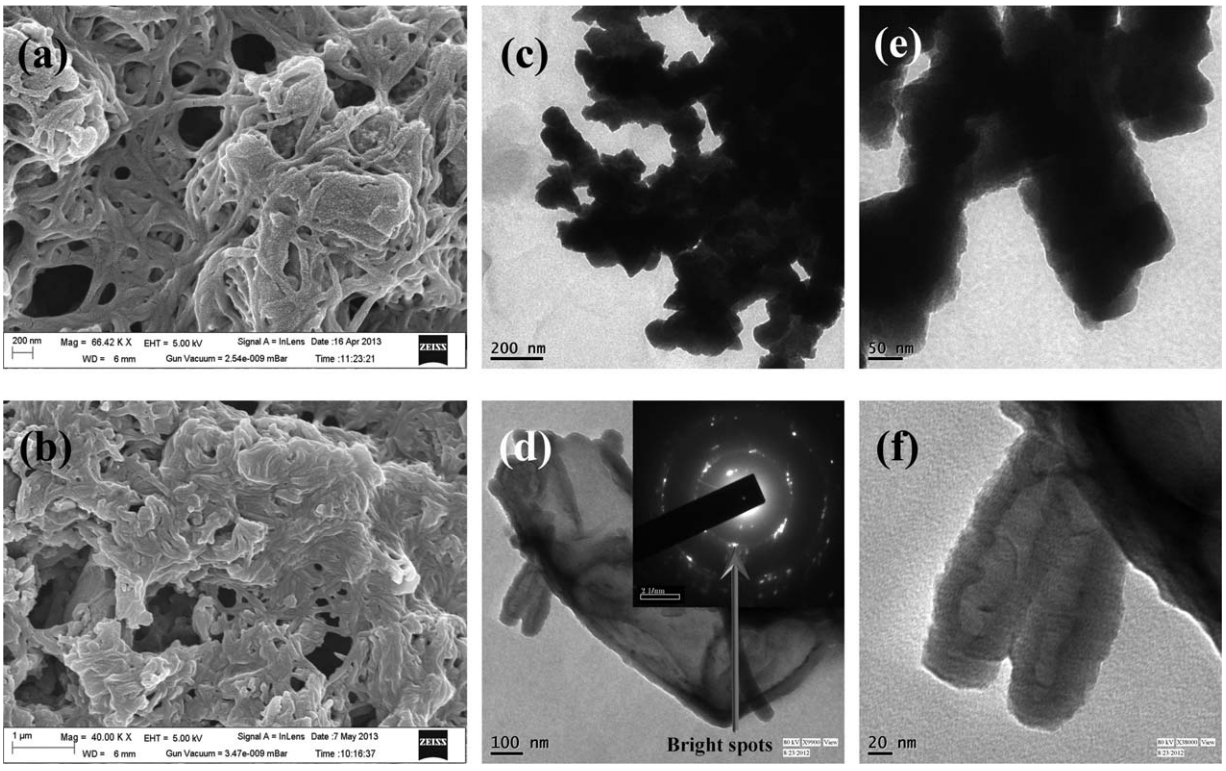

Figure 1. (a,b) FESEM and (c–f) HRTEM pictures of individually doped PAni. (a,c,e) PS_0T_4 (PTSA doped) and (b,d,f) PS_4T_0 (H_2SO_4 doped). (e,f) Magnified HRTEM pictures. (d) Inset: SAED pattern of PS_4T_0.

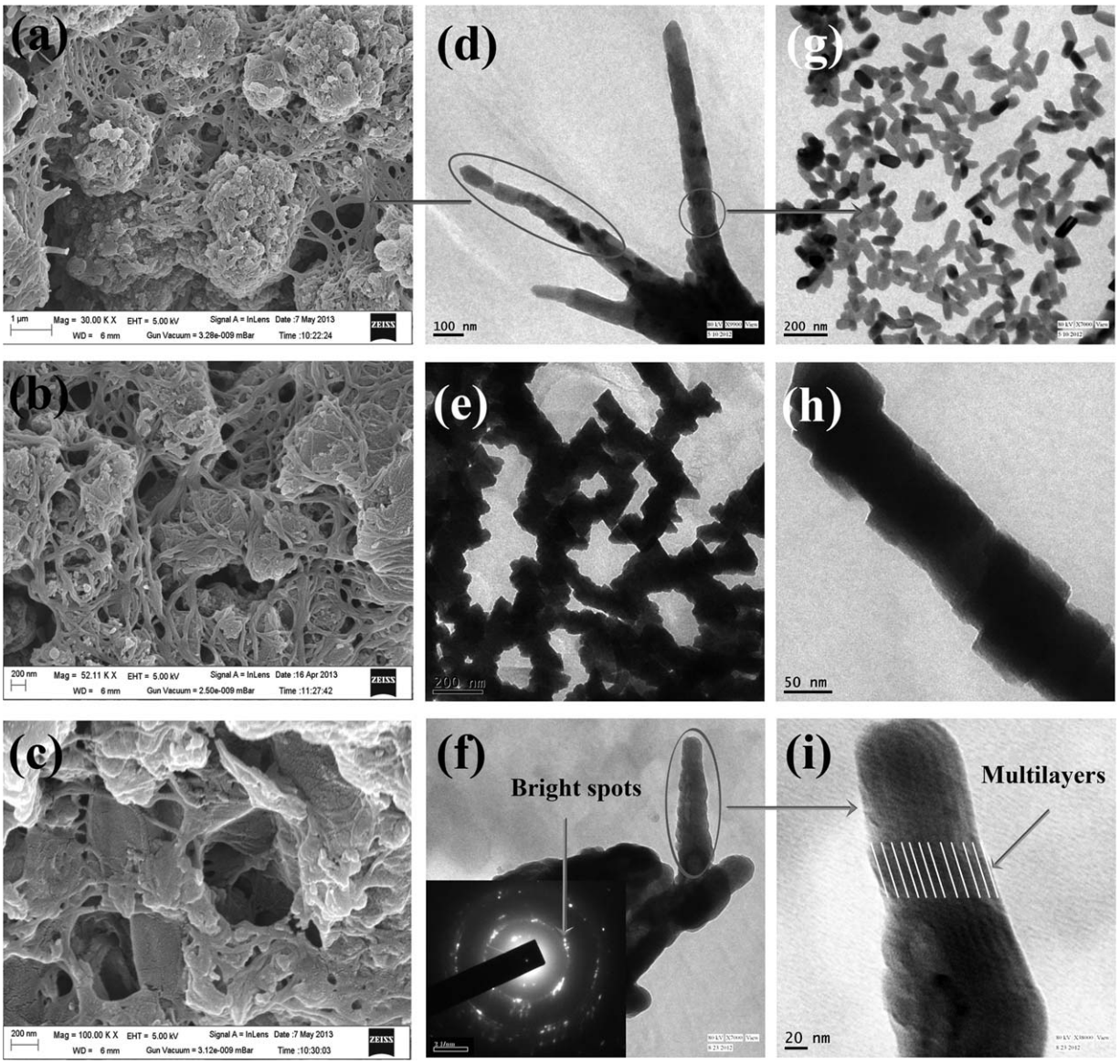

Figure 2. (a–c) FESEM and (d–i) HRTEM pictures of simultaneously dual doped PAni. (a,d,g) PS_1T_3 with $[H_2SO_4]$: [PTSA] = 1 : 3 (b,e,h) PS_2T_2 with $[H_2SO_4]$: [PTSA] = 1 : 1 and (c,f,i) PS_3T_1 with $[H_2SO_4]$: [PTSA] = 3 : 1 (c,f,i). (g,h,i) Magnified HRTEM pictures. (f) Inset: SAED pattern of PS_3T_1.

Synthesis

Aniline sulfate was prepared from reaction of aniline with sulfuric acid. Electrochemical polymerization of polyaniline was performed from 0.5*M* aniline sulfate in DMF medium in a single compartment cell. Simultaneous dual doping *in situ* with synthesis process was performed using H_2SO_4 and PTSA keeping the total dopant concentration constant at 1*M*. The ratio of the concentration of $[H_2SO_4]$: [PTSA] was varied at 1 : 3, 1 : 1, and 3 : 1. During synthesis, constant current of 0.05 Å between the electrodes was applied for an hour, thereafter the polarity of the electrodes was changed and the process continued for 30 min. The whole process was further repeated twice. The final products were rinsed and filtered with deionized water, methanol, and ethanol to eliminate the oligomers followed by drying at 60°C for 15 min. Samples are designated as PS_mT_n where P stands for PAni, S indicates sulfuric acid, PTSA is denoted by T, and the ratio of the subscript numbers (m : n) represents the molar ratio of the two dopants used for synthesis of PAni. All the sample designations of synthesized PAni are listed in Table I.

Characterizations

AC resistance was measured from PAni pellets with Quadtech 7600 Precision LCR Meter (Model—B) using circular copper plate electrodes. AC conductivity was calculated using the equation $\sigma = t/(A.R)$ where σ is conductivity (S), t is the thickness of the sample (cm), A is the area of the electrode (3.8476 cm^2), and R is the measured resistance (Ω). FTIR spectra of the PAni samples were recorded using a Perkin-Elmer (model—Spectrum RX1) FTIR spectrometer, Spectrum RX 1 using KBr pellet of

PAni. XRD was performed with Cu target using an X-ray wavelength of 1.54 Å operated at 40 kV and 40 mA. FESEM was done in Supra 40, Carl Zeiss, Germany at accelerating voltage of 5 kV. Ultrasonicated PAni powder samples were dispersed on the surface of smooth glass slide and gold coating was performed prior to FESEM analysis. HRTEM was performed in JEOL JEM 2100 instrument at accelerating voltage of 80 kV. Thermogravimetric analysis (TGA) was performed using TGA, Q 50 (TA Instruments) in nitrogen atmosphere from room temperature to 630°C at 20°C/min heating rate. Cyclic voltammetry was performed in Autolab Electrochemical Workstation 302N instrument in the potential window of −0.2 to +1.0 V (vs. Ag/AgCl) at 5 mV/s scan rate using platinum disc working electrode, platinum rod counter electrode and 1*M* H_2SO_4 as electrolyte. Gravimetric-specific capacitance was calculated from the equation[35]:

$$C_s = \frac{Q_a + |Q_c|}{2mv(E_2 - E_1)} = \frac{\int_{E_1}^{E_2} I_a(E)dE + \left|\int_{E_2}^{E_1} I_c(E)dE\right|}{2mv(E_2 - E_1)},$$

where C_s is the gravimetric specific capacitance, Q_a and Q_c are the respective charges during anodic and cathodic cycle, E_2 and E_1 are the upper and lower limit of the potential window, I_a and I_c are the respective currents during anodic and cathodic scan, m is the mass of the sample, and v is the scan rate.

RESULTS AND DISCUSSION

To have an insight into structural features of polyaniline, both surface and bulk morphologies were thoroughly investigated for PAni doped with single dopant (Figure 1) as well as with double dopants (Figure 2). Self-assembled nano and microporous mesh-like structures are found to form during the course of synthesis [Figures 1(a,b) and 2(a–c)]. Interconnected nanosized wires form mesh-like structures consisting of voids along with solid clusters devoid of pores. A closer view of surface morphology reveals that these clusters are formed due to agglomeration and aggregation of the nanowires. Diameter of the nanowires ranges between 25 and 140 nm. The histogram of size (diameter) distributions of synthesized PAni nanowires is shown in Figure 3. Nanowire diameter changes with the change in relative concentration of H_2SO_4 with respect to PTSA. For dual doped PAni, average diameters of both PS_2T_2 and PS_3T_1 are less than both of the individually doped PAni. But, an increase in diameter is observed for highly PTSA doped PS_1T_3 which is even higher than only PTSA doped sample PS_0T_4. Although the surface morphology of PAni samples appears to be similar for both individual and dual doped samples, the bulk morphology revealed from HRTEM analysis exhibits the effect of dopants on nanostructure formation. The mechanism for the formation of nanowire using different dopant concentrations has been explained in Scheme 1. Neat PTSA doping (PS_0T_4) results in formation of small particles having sharp edge, which combine together, often directionally to form wire-like structure. This also happened for dual doped $PS_1T_3$and PS_2T_2. On the contrary, both neat H_2SO_4 doped sample PS_4T_0 and dual doped PS_3T_1 show formation of thin layered structure leading to multilayered tube formation. Wider part of the nanolayers in PS_4T_0 possibly folds around to give the shape of nanowires of smaller diameter

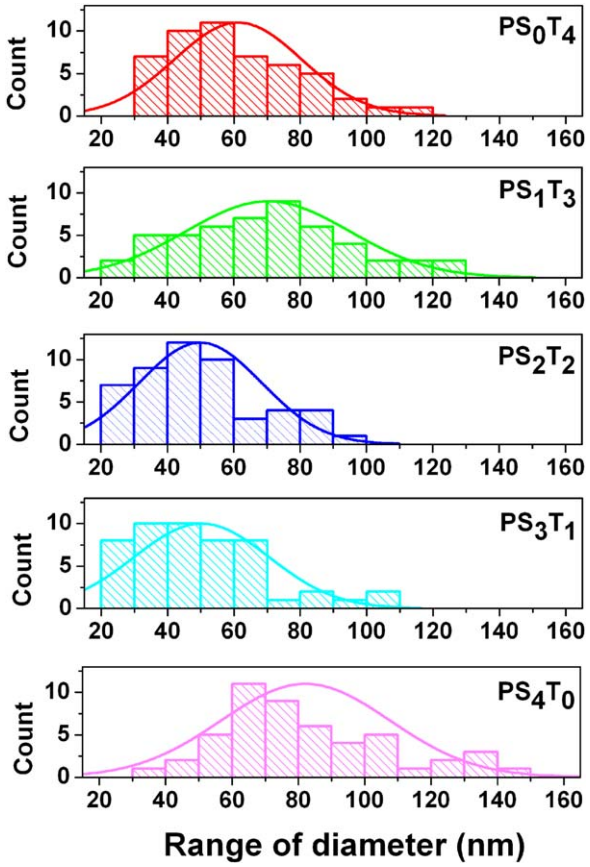

Figure 3. Histograms of diameter distribution of PAni nanowires measured at 50 different points of FESEM images. [Color figure can be viewed in the online issue, which is available at wileyonlinelibrary.com.]

and the similar mechanism may happen for PS_3T_1 also. This phenomenon finds resemblance with the formation of tubular structure from PAni nanosheets of thickness 30–100 nm as reported by Zujovic et al.[36] where the decrease of free surface energy was suggested as the driving force for the "rolling-up" mechanism proposed for such structural transformation. Here,

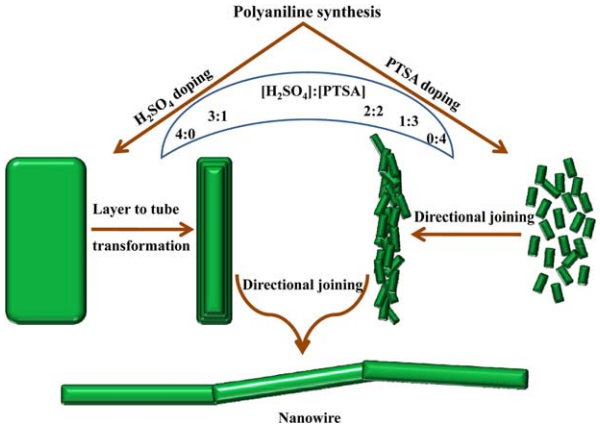

Scheme 1. Schematic representation of nanostructure formation and transformation to nanowire for individually and dual doped PAni synthesized in DMF medium. [Color figure can be viewed in the online issue, which is available at wileyonlinelibrary.com.]

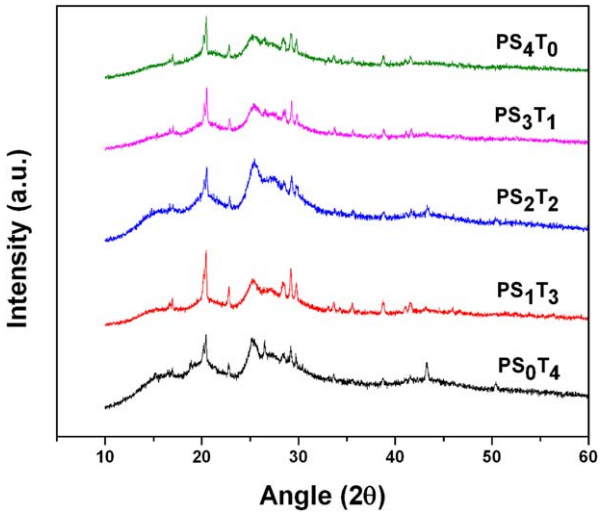

Figure 4. X-ray diffractograms of individually and dual doped PAni. [Color figure can be viewed in the online issue, which is available at wileyonlinelibrary.com.]

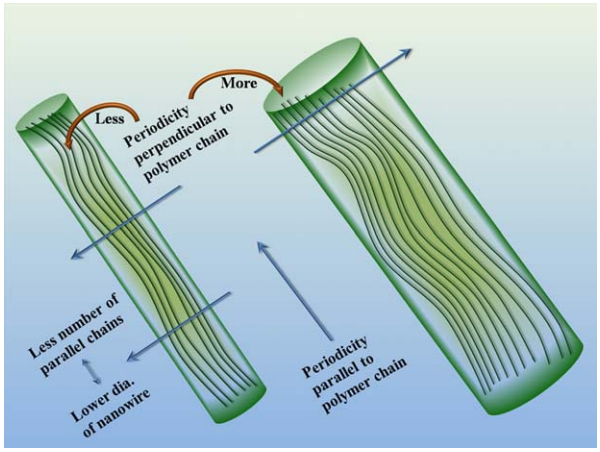

Scheme 2. Schematic representation of correlation between diameter of PAni nanowire (from FESEM) and periodicity perpendicular to polymer chain (from XRD). [Color figure can be viewed in the online issue, which is available at wileyonlinelibrary.com.]

in this work, the galvanostatic condition of electrochemical synthesis may play a role in the transformation from layer to tubular structure which needs further investigation to establish any comprehensive mechanism for such phenomenon. The inter-layer distance [the layers are highlighted with white lines in Figure 2(i)] in the multilayered tubes varies between 5 and 8 nm for PS_3T_1, which is even lower in PS_4T_0 to the range of 2–3 nm [Figure 1(f)] suggesting more compactness of the layers. The wider inter-layer distance for PS_3T_1 compared to PS_4T_0 may be attributed to the plasticizing effect of PTSA. Multilayered morphology is formed in PS_4T_0 in presence of H_2SO_4. As the proportion of PTSA increases beyond PS_3T_1 towards PS_0T_4, bigger size of PTSA anion compared to sulfate ion may hinder the formation of layers, rather it leads to the formation of small nanoparticles. Thus, a change in the transformation from particles or layers to nanowire-like structures takes place with the change in the ratio of the dopants. Formation of different nanostructures with changing the type and concentration of dopants is a well-known fact, and the same has also been reported for PTSA doping by several researchers.[37–39] SAED pattern [Figure 1(d) inset] of PS_4T_0 and [Figure 2(f) inset] of PS_3T_1 shows polycrystalline rings with multiple bright spots which indicates the presence of both ordered and disordered multilayers.[40,41] In our previous work[25] with the similar dopant combination performed in aqueous medium instead of DMF, agglomerated macro-sized spherical surface morphology was observed for all combinations unlike nanowires as observed in this investigation. Apart from that, in the said work nanosized flakes/layers were found for doping with H_2SO_4, nearly spherical morphology was exhibited for doping with PTSA whereas, nanorods with smooth surface were revealed for dual doped PAni at $[H_2SO_4] : [PTSA] = 3 : 1$. Thus, this investigation reveals that the presence of aprotic polar solvent like DMF as electrolyte medium instead of water (a protic polar solvent) is playing an important role in the formation of nanostructures with some differences as well as in the transformation to nanowire-like structures. Because of the absence of labile protons in aprotic polar electrolyte, the dissociated dopant anions are not solvated by formation of hydrogen bonding. Thus, the naked anions may dope more effectively in case of DMF compared to water as electrolyte. Although the

Table II. Ratio of Intensities of XRD Peaks ($2\theta = 20.4°$ and $25.4°$) and Benzenoid to Quinonoid Ratios (B : Q) Calculated from FTIR Spectrographs of PAni

Sample code	Intensity ratio ($I_{20.4}/I_{25.4}$) [XRD]	B : Q ratio [FTIR]
PS_0T_4	1.018	55 : 45
PS_1T_3	1.182	62 : 38
PS_2T_2	0.975	55 : 45
PS_3T_1	1.046	82 : 18
PS_4T_0	1.047	70 : 30

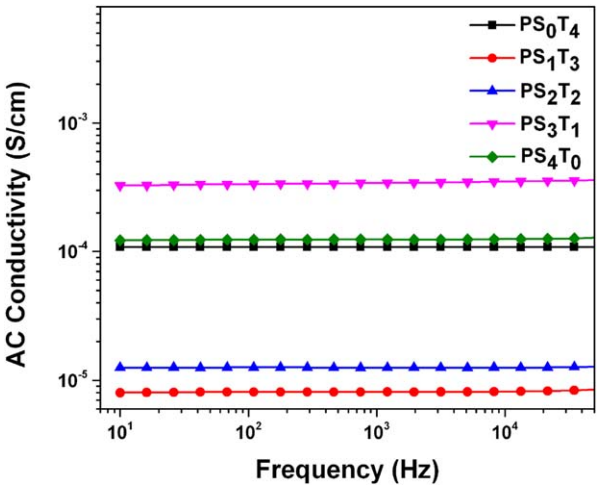

Figure 5. AC conductivity of individually and dual doped PAni showing synergistic improvement in PS_3T_1. [Color figure can be viewed in the online issue, which is available at wileyonlinelibrary.com.]

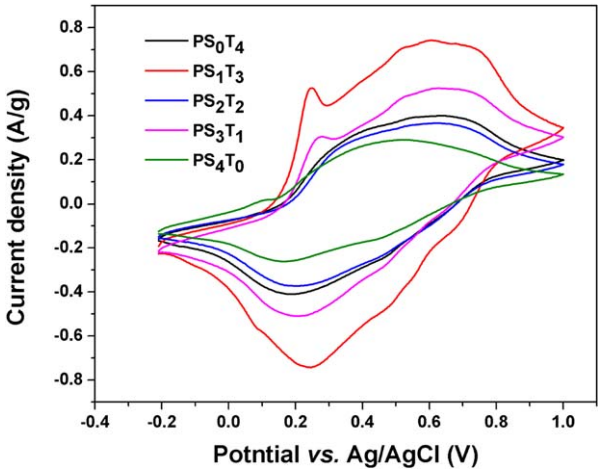

Figure 6. Cyclic voltammograms performed at 5 mV/s scan rate within the potential window of −0.2 to 1.0 V (vs. Ag/AgCl) using 1*M* H_2SO_4 electrolyte. [Color figure can be viewed in the online issue, which is available at wileyonlinelibrary.com.]

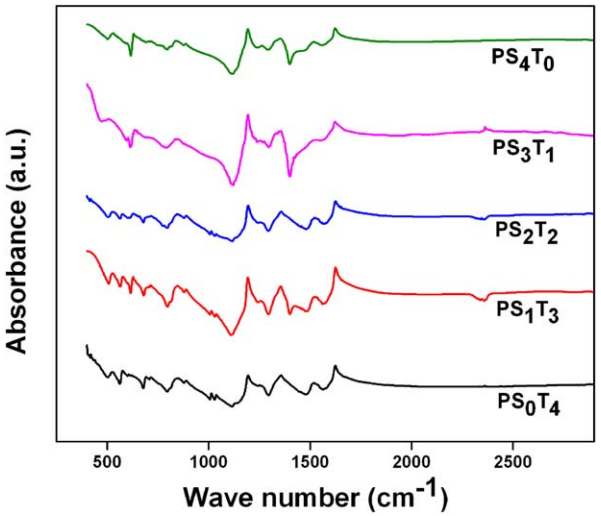

Figure 7. FTIR spectra of individually and dual doped PAni. [Color figure can be viewed in the online issue, which is available at wileyonlinelibrary.com.]

formation mechanism of the multilayers and the directional joining behavior of nanoparticles need further investigation for better understanding, it may be suggested that the nanostructure formation mechanism may not be attributed to progressive and instantaneous nucleation followed by 2D and 1D growth, respectively, as reported in early literatures.[42,43] Rather, the 2D propagation of polymer chains forming layered structure for dopant anions with smaller ionic radius (for H_2SO_4 doping) and directional joining of particles for dopant ions with larger ionic radius (for PTSA doping) may be attributed to complex nucleation process in DMF medium. Again, the plasticizing effect of PTSA may increase the inter-layer distance for PS_3T_1 compared to PS_4T_0.

In XRD patterns of different samples, two broad peaks are observed at $2\theta \sim 20.4°$ and 25.4° (Figure 4). The peak centered at $2\theta \sim 20.4°$ is ascribed to periodicity parallel to the polymer chain, and the latter is due to the periodicity perpendicular to the polymer chain.[14] The ratio of peak height at $2\theta = 20.4°$ and 25.4° is shown in Table II. The increase in intensity ratio for PS_1T_3 indicates the increase in periodicity parallel to polymer chain, whereas the decrease in this ratio for PS_2T_2 signifies the increase in periodicity perpendicular to the polymer chain. In addition, the diameter of PS_1T_3 is also wider than PS_0T_4, PS_2T_2, and PS_3T_1 (Figure 3) which is interesting to find some correlation between these two parameters. It is generally considered

Table III. Gravimetric Specific Capacitance of Synthesized PAni

Sample	Gravimetric specific capacitance at 5 mV/s scan rate (F/g)
PS_0T_4	54.29
PS_1T_3	98.45
PS_2T_2	49.42
PS_3T_1	71.95
PS_4T_0	38.19

that the polymer chains are aligned axially along the nanowires and the increase in the number of such polymer chains in radial direction increases the diameter of nanowires (Scheme 2). Thus, with the increase in diameter, periodicity perpendicular to polymer chain increases compared to periodicity parallel to polymer chain. Presence of some extent of crystallinity is evident from presence of small sharp peaks.

Electrical property was characterized by AC conductivity (Figure 5). Frequency-independent nature for all PAni samples as revealed in this investigation is a characteristic of conducting polymer. AC conductivity of PS_4T_0 and PS_0T_4 is found to be of very close values (Figure 5). In PS_1T_3 and PS_2T_2, AC conductivity decreases from both individually doped PAni. On the contrary, conductivity of PS_3T_1 was found to be even higher than both individually doped PAni samples, inferring synergy in this

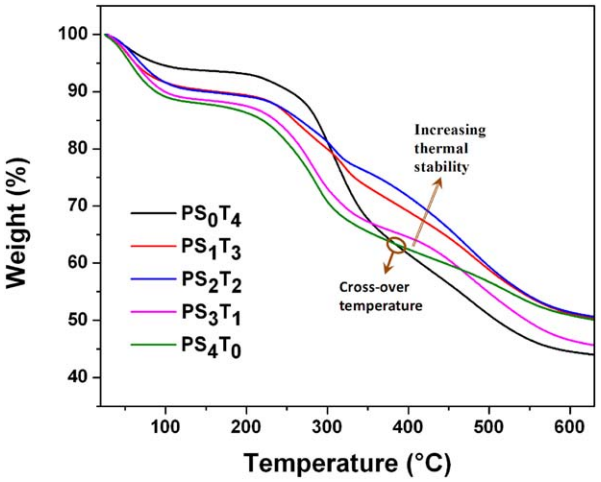

Figure 8. Thermogravimetric analysis of PAni showing synergistic effect of dopants in thermal degradation within particular temperature range. [Color figure can be viewed in the online issue, which is available at wileyonlinelibrary.com.]

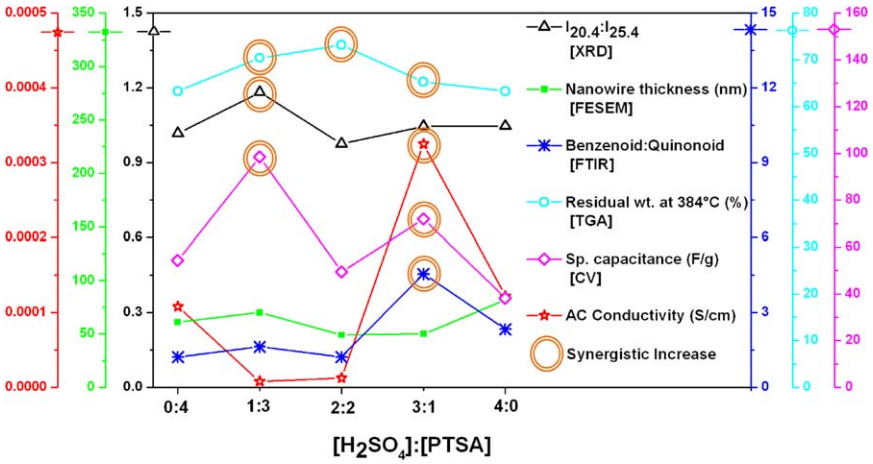

Figure 9. Variations of different properties and measured parameters for PAni with the change in dopant ratio. Circular markings indicate synergistic increase in measured parameters or properties for dual doped PAni compared to the individually doped samples. [Color figure can be viewed in the online issue, which is available at wileyonlinelibrary.com.]

property. Relative position of the dopants and their arrangement may increase or decrease the difference in polarity locally in the polymer chain which in turn results in respective synergistic increase or decrease in conductivity.

Electroactivity of synthesized PAni is evident from cyclic voltammograms (Figure 6). Quasi-rectangular shape of voltammograms indicates capacitative behavior of different samples. Although all three pairs of expected redox peaks[44] due to interconversion of different oxidation states (leucoemeraldine, pernigraline, and emeraldine) are not prominent for all samples, but these are more strongly visible for dual doped samples PS_1T_3 and PS_3T_1. Gravimetric specific capacitances (C_s) calculated from voltammograms are shown in Table III. The sample PS_2T_2, doped with equal proportion of two dopants has gravimetric specific capacitance 49.42 F/g. This is intermediate between the values of capacitance obtained for PAni doped with single dopant. Specific capacitance of PS_1T_3 and PS_3T_1 are 98.45 and 78.95 F/g, respectively. This indicates the synergistic effect of dual dopants in the improvement of specific capacitance compared to the effect of single dopant. As the enhancement in conductivity favors the dissipation of charge stored in the material, increment in capacitative behavior along with the decrease in AC conductivity is observed for PS_0T_4 and PS_3T_1 as compared to PS_4T_0 and PS_1T_3, respectively. Although PS_1T_3 exhibits the highest specific capacitance, its AC conductivity is even less than either of the singly doped PAni. Therefore, optimized effect of synergism for the improvement of both electrical and electrochemical property is achieved for PS_3T_1.

FTIR spectra of different PAni are given in Figure 7. The absorption band at 1294 cm^{-1} may be ascribed to π electron delocalization induced in the polymer through protonation or C—N—C stretching vibration. The absorption peak at 1244 cm^{-1} is the characteristic of C—N stretching vibration in the polaron structure. The band at 1114 cm^{-1} is assigned to the vibration mode of the —NH in the protonated emeraldine base (B—NH^+=Q). The band at 795 cm^{-1} is due to C—H out of plane deformation of 1,4-disubstituted benzene rings. The characteristic peaks due to benzenoid (B) and quinonoid (Q) ring stretching appear near 1480 cm^{-1} and 1560 cm^{-1} [33,45] which is the confirmatory evidence for the formation of partially oxidized and partially reduced emeraldine form of PAni. In all these cases, benzenoid structure predominates over quinonoid one. B : Q ratio (Table II) was calculated from the ratio of the area under corresponding peaks and it changes abruptly with the use of both the dopants simultaneously. B : Q ratio reaches the highest value of 82 : 18 in the case of PS_3T_1 which also exhibits the highest AC conductivity (Figure 5). For other two dual doped PAni the B : Q ratio lies in between those of PS_0T_4 and PS_4T_0 which also show lower AC conductivity than either of the two singly doped PAni. The mechanism of abrupt increase in B : Q ratio in PS_3T_1 is yet to be fully understood, but some correlation may exist with the synergistic effect of dual doping on AC conductivity.

Thermogravimetric analysis (Figure 8) shows three-stage degradation for all types of doped PAni. The first stage of degradation near 100°C is due to removal of moisture which decreases with the increase in the proportion of PTSA in the total dopant concentration. Moisture content for H_2SO_4 doped PS_4T_0 only is as high as ~11%, whereas in only PTSA doped PS_0T_4 it is only 6%. The second stage of degradation occurring in between 200 and 300°C may be ascribed to removal of dopants followed by polymer chain degradation in the third stage near 400°C. Up to 384°C, PS_0T_4 shows higher thermal stability compared to PS_4T_0,[19] but the trend changes beyond this temperature. Synergistic improvement in thermal degradation (i.e., less degradation) is observed in dual doped PAni near the cross-over temperature (384°C) which may be due to absorption of more energy by the combination of dopants. A part of the absorbed energy may be dissipated in the relative rearrangement of the dopants which allows less energy to be used for degradation. Such synergy is in agreement with enhancement in thermal stability due to codoping reported

earlier[33] and is best observed in PS_2T_2 which shows ~10% less weight loss at the cross-over temperature of 384°C. Probable reason of the highest thermal stability of PS_2T_2 is the presence of equimolar amount of dopants where the scope of their rearrangement upon thermal excitation and consequent heat dissipation is the maximum.

Considering all the above-mentioned observations, a comparative representation of different properties and measured parameters from different characterizations are shown in Figure 9. This figure clearly indicates synergistic increase in different properties for dual doped PAni which is dominant for unequal proportion of dopants.

CONCLUSIONS

Nanostructured polyaniline was electrochemically synthesized using PTSA and H_2SO_4 to produce different samples containing both dual doped as well as singly doped system. Monitoring of nanostructure reveals transformation of different smaller nanostructures to similar nanowires. Diameters of the nanowires formed can be correlated with periodicity of polymer chains along both axial and radial direction in nanowires. Synergistic improvement in both AC conductivity and specific capacitance is observed for dual doped system. Specific capacitance is the highest for $[H_2SO_4] : [PTSA] = 1 : 3$, whereas synergistic improvement in both electrical and electrochemical properties is optimized for $[H_2SO_4] : [PTSA] = 3 : 1$. Within certain temperature range, mixed dopant system exhibits less thermal degradation.

REFERENCES

1. Matveeva, E. S.; Calleja, R. D.; Sanchez-Martinez, E. *Synth. Met.* **1994**, *67*, 207.
2. Gosh, M.; Barman, A.; Meikap, A. K.; De, S. K.; Chatterjee, S. *Phys. Lett. A* **1999**, *260*, 138.
3. Sutar, D. S.; Tewari, R.; Dey, G. K.; Gupta, S. K.; Yakhmi, V. J. *Synth. Met.* **2009**, *159*, 1067.
4. Li, J.; Fang, K.; Qi, H.; Li, S.; Mao, W. *Synth. Met.* **2004**, *142*, 107.
5. Wang, H.; Hao, Q.; Yang, X.; Lu, L.; Wang, X. *Electrochem. Commun.* **2009**, *11*, 1158.
6. Gupta, V.; Miura, N. *Mater. Lett.* **2006**, *60*, 1466.
7. Pattananuwat, P.; Aht-Ong, D. *Adv. Mater. Res.* **2010**, *93–94*, 459.
8. Sadek, A. Z.; Wlodarski, W.; Kalantar-Zadeh, K.; Baker, C.; Kaner, R. B. *Sensor Actuat. A-Phys.* **2007**, *139*, 53.
9. He, L.; Jia, Y.; Menga, F.; Li, M.; Liu, J. *Mater. Sci. Eng. B* **2009**, *163*, 76.
10. Jeyaprabha, C.; Sathiyanarayanan, S.; Venkatachari, G. *J. Appl. Polym. Sci.* **2006**, *101*, 2144.
11. Koul, S.; Chandra, R.; Dhawan, S. K. *Polymer* **2000**, *41*, 9305.
12. Jung, W. H.; Lee, Y. M.; Jo, N. J.; Lee, J. O. *Macromol. Chem. Phys.* **2008**, *209*, 1083.
13. Tang, Z.; Liu, S.; Wang, Z.; Dong, S.; Wang, E. *Electrochem. Commun.* **2000**, *2*, 32.
14. Li, J.; Jia, Q.; Zhu, J.; Zheng, M. *Polym. Int.* **2008**, *57*, 337.
15. Du, X. S.; Zhou, C. F.; Wang, G. T.; Mai, Y. W. *Chem. Mater.* **2008**, *20*, 3806.
16. Angelopoulos, M.; Dipietro, R.; Zheng, W. G.; MacDiarmid, A. G.; Epstein, A. J. *Synth. Met.* **1997**, *84*, 35.
17. Bhadra, S.; Singha, N. K.; Chattopadhyay, S.; Khastgir, D. *J. Polym. Sci. Part B: Polym. Phys.* **2007**, *45*, 2046.
18. Abdiryim, T.; Jamal, R.; Nurulla, I. *J. Appl. Polym. Sci.* **2007**, *105*, 576.
19. Dhawan, S. K.; Singh, N.; Rodrigues, D. *Sci. Technol. Adv. Mater.* **2003**, *4*, 105.
20. Li, J.; Fang, K.; Qiu, H. *Synth. Met.* **2004**, *142*, 107.
21. Palaniappan, S.; Devi, S. L. *J. Appl. Polym. Sci.* **2008**, *107*, 1887.
22. Tigelaar, D. M.; Lee, W.; Bates, K. A.; Saprigin, A.; Prigodin, V. N.; Cao, X.; Nafie, L. A.; Platz, M. S.; Epstein, A. J. *Chem. Mater.* **2002**, *14*, 1430.
23. MacDiarmid, A. G.; Epstein, A. J. *Synth. Met.* **1994**, *65*, 103.
24. Palaniappan, S.; Rajender, B. *Adv. Synth. Catal.* **2010**, *352*, 2507.
25. Bhandari, S.; Singha, N. K.; Khastgir, D. *J. Appl. Polym. Sci.* **2013**, *29*, 1264.
26. Kim, S. H.; Oh, K. W.; Choi, J. H. *J. Appl. Polym. Sci.* **2010**, *116*, 2601.
27. Han, J.; Fang, P.; Dai, J.; Guo, R. *Langmuir* **2012**, *28*, 6468.
28. Guo, X.; Fei, G. T.; Su, H.; Zhang, L. D. *J. Phys. Chem. C* **2011**, *115*, 1608.
29. Konyushenko, E. N.; Stejskal, J.; Sedenkova, I.; Trchova, M.; Sapurina, I.; Cieslar, M.; Prokes, J. *Polym. Int.* **2006**, *55*, 31.
30. Qunwei, T.; Xiaoming, S.; Qinghua, L.; Jihuai, W.; Jianming, L.; Miaoliang, H. *Mater. Lett.* **2009**, *63*, 540.
31. Armes, S. P.; Aldissi, M.; Agnew, S.; Gottesfeld, S. *Mol. Cryst. Liq. Cryst.* **1990**, *190*, 63.
32. Hou, X.; Schober, M.; Chu, Q. *Cryst. Growth Des.* **2012**, *12*, 5159.
33. Roy, S.; Kargupta, K.; Chakraborty, S.; Ganguly, S. *Mater. Lett.* **2008**, *62*, 2535.
34. Arenas, M. C.; Sanchez, G.; Nicho, M. E.; Elizalde-Torres, J.; Castano, V. M. *Appl. Phys. A* **2012**, *106*, 901.
35. Gao, Y.; Pandey, G. P.; Turner, J.; Westgate, C. R.; Sammakia, B. *Nanoscale Res. Lett.* **2012**, *7*, 651.
36. Zujovic, Z. D.; Laslau, C.; Bowmaker, G. A.; Kilmartin, P. A.; Webber, A. L.; Brown, S. P.; Travas-Sejdic, J. *Macromolecules* **2010**, *43*, 662.
37. Rashid, M.; Rahim, A. A.; Noordin, M. J. *Anti-Corros. Methods Mater.* **2011**, *58*, 131.
38. Wu, J.; Sun, Y.; Xu, W.; Zhang, Q. *Synth. Met.* **2014**, *189*, 177.

39. Choi, J. H.; Kim, S. H.; Oh, K. W. *Mol. Cryst. Liq. Cryst.* **2007**, *464*, 281/[863].

40. Nepal, A.; Singh, G. P.; Flanders, B. N.; Sorensen, C. M. *Nanotechnology* **2013**, *24*, 245602.

41. Sun, Z.; Dong, N.; Wang, K.; Konig, D.; Nagaiah, T. C.; Sanchez, M. D.; Ludwig, A.; Cheng, X.; Schuhmann, W.; Wang, J.; Muhler, M. *Carbon* **2013**, *62*, 182.

42. Bade, K.; Tsakova, V.; Schultze, J. W. *Electrochim. Acta* **1992**, *37*, 2255.

43. Kemp, N. T.; Cochrane, J. W.; Newbury, R. *Synth. Met.* **2009**, *159*, 435.

44. Gomez, H.; Ram, M. K.; Alvi, F.; Villalba, P.; Stefanakos, E. L.; Kumar, A. *J. Power Sources* **2011**, *196*, 4102.

45. Trchova, M.; Sedenkova, I.; Tobolkova, E.; Stejskal, J. *Polym. Degrad. Stab.* **2004**, *86*, 179.